11

Multilayer Antireflective Composite Nanocoatings for Protective Glass in Optical Sensors

© M.Yu. Vasilkov[1,2], I.D. Kosobudskii[1], N.M. Ushakov[1,2,¶]

[1] Saratov Branch, Kotelnikov Institute of Radio Engineering and Electronics, Russian Academy of Sciences, Saratov, Russia
[2] Saratov National Research State University, Saratov, Russia

[¶] e-mail: nmu@bk.ru

Received October 02, 2025
Revised November 07, 2025
Accepted November 27, 2025

Multilayer mesoporous composite antireflective coatings SiO_2@ZnO and SiO_2@TiO_2 for glass plates with different optical refractive indices (1.52 and 1.8) were developed using sol-gel technology. The resulting sols were applied to glass plates by dip-coating from a solution at $23 \pm 10\,^{\circ}$C. The extraction rate from the solution was varied from 100 to 180 mm/min. Glass plates with coatings applied to both sides were dried at room temperature until a film formed and then heat-treated in a muffle furnace at $500\,^{\circ}$C. During annealing, a composite composition of SiO_2@ZnO and SiO_2@TiO_2 films was formed. The thickness of the SiO_2 layer ranged from 100 ± 5 to 120 ± 5 nm, depending on the experimental conditions. The composite layer thicknesses were: SiO_2@ZnO 100 ± 10 nm, SiO_2@TiO_2 to 140 ± 5 to 185 ± 5 nm. The results of measuring the reflectance and transparency spectra of glass with single-, two-, and three-layer coatings made of sols with different compositions and drawing rates are presented. It is shown that two-layer mesoporous composite coatings with different compositions best demonstrate the antireflective properties of glass with medium (1.52) and high (1.8) refractive indices over a wide optical range of 400−1000 nm.

Keywords: sol-gel technology, SiO_2@ZnO(TiO_2) composition, mesoporous antireflective coating, multilayer composite coating, protective glass.

DOI: 10.61011/EOS.2026.02.63469.8610-25

Introduction

To improve the efficiency of solar energy conversion by optical instruments made of multi-element lenses, the optical lenses may be reduced considerably, using the dependence of the reflectivity on the phase changes and the refractive index. This may be achieved by covering the optical surface with thin, transparent and dielectric layers called antireflection coatings (ARC), which have certain values of the refractive index and thickness. Antireflective coatings reduce losses for Fresnel reflection and therefore improve light transmission. ARCs are widely used in various applications, such as display panels, solar elements and optical lenses [1].

High efficiency of multi-layer antireflection coatings may be achieved by reduction of the refractive index of the upper layer and formation of a finely structured porous film. Papers are known, where thin films of porous SiO_2 with super-low refractive indices and two-layer antireflection coatings with broadband, highly transmissive and scratchproof properties were obtained by simple sol-gel method [2–4]. Sol-gel synthesis is carried out at relatively low temperatures and makes it possible to obtain the materials that are homogeneous in their structure and properties and also makes it possible to easily introduce particles of various nature into their composition. Porous films hold a specific place among the thin-film coatings. Porosity (ratio of the volume of cavities in the material to its total volume) influences the properties and application of the films. Porous materials are classified by pore size: microporous (pore size up to 2 nm), mesoporous (pore size from 2 to 50 nm), macroporous (pore size of more than 50 nm). Thin films with high content of pores are necessary to create the materials characterized by low dielectric constant, low refractive index and low thermal conductivity. Porous materials have large interface, high volume of pores, colloidal stability, inertness and wide opportunities of chemical modification of the inner surface of the pores [5,6].

Structured and porous materials become promising optical materials [7,8].

Theoretically, to reduce to zero the reflection of light from the glass with the refractive index $n_g \sim 1.52$ at wavelength λ_0, a transparent film coating is necessary with low refractive index ($n = \sqrt{n_g} \approx 1.23$) and thickness $\lambda_0/4$ [9]. Film-forming materials with such low refractive index is nonexistent in nature. Therefore, in practice of elucidation of optical parts, multilayer coatings produced with vacuum technology have become widely used. However, the main disadvantage of vacuum technology is the use of expensive equipment, and the dimensions of the used substrate are limited by the dimensions of the vacuum chamber in the sputtering apparatus. As the dimensions of the substrate increase, the cost of the sputtering processes increases as

well. As the alternative method of elucidation, recently single- and multilayer porous composite film coatings have been proposed, which are produced by chemical methods, in particular, using sol-gel technology [10,11]. The structure of such multilayer elucidating coatings provides for the combination of the layers with high and low refractive indices. Materials with high refractive index are, for example, TiO_2 (2.6), SnO_2 (2.0), CeO_2 (1.95) and others. Materials with low refractive index are, for example, SiO_2 (1.45), MgF_2 (1.38) and others. Materials with medium refractive index (1.5−1.9) are Al_2O_3 (1.77), LaF_3 (1.54), CeF_3 (1.57) and others. Therefore, porous coatings based on such materials as SiO_2 and TiO_2 are of scientific and practical interest.

Single-layer coatings made of composite silicate mesoporous materials SiO_2@CuO and SiO_2@ZnO, developed on the basis of sol-gel technological methods in paper [12] have shown their efficiency for improvement of glass transparency, but with limited broadbandness. it is possible to achieve the considerable increase in broadbandness without substantial reduction in the optical transparence on the basis of multilayer mesoporous coatings. In paper [13] a two-layer coating was developed on the basis of SiO_2@TiO_2 naterials. A glass substrate was coated with a layer of mesoporous SiO_2 using the method of acid catalysis, the second layer from mesoporous TiO_2 was applied by dipping method. Light transmission was 96.9% ($\lambda = 620$ nm). Such coatings have demonstrated good hydrophilic properties due to the presence of TiO_2. In paper [14] optimized two-layer quarter-wave antireflection coatings SiO_2/TiO_2, SiO_2/Al_2O_3, SiO_2/*anatase* TiO_2 and SiO_2/*rutile* TiO_2 were developed using TFCalc software to design thin films. Coatings SiO_2/TiO_2 were made using sol-gel method in accordance with the developed optimal parameters. It is interesting that in the manufactured coatings SiO_2/TiO_2 simultaneously the properties of abrasive resistance and broadbandness were found, which makes this coating system SiO_2/TiO_2 promising for real applications in optical and display devices.

Therefore, the purpose of this paper was development of multilayer broadband elucidating composite coatings on the basis of silicate mesoporous materials SiO_2/SiO_2@ZnO and SiO_2/SiO_2@TiO_2.

Materials and methods

In this paper the study objects were composite two-layer and three-layer nanocoatings based on porous silicon dioxide SiO_2 and silicon dioxide modified with zinc oxide ZnO or titanium dioxide TiO_2 applifed on the surface of object slides (75×25×1.1 mm, ApexLab, Russian Federation) by method of pulling from sol solution. Initially a layer of SiO_2 was applied on the slides with variable thickness d_1 (at pulling speed 110−168 mm/min) from the formed sol of silicon dioxide prepared by sequential mixing of distilled water, ethyl alcohol, acetic acid and tetraethoxysilane at mole ratio of 12.2 : 30 : 2 : 1. After application of the coating on the basis of SiO_2 the substrate was thermally treated in air atmosphere at 500 ± 5 °C for 30 min, then the second layer of SiO_2@ZnO coating was applied with thickness of d_2 from sol with composition similar to the above, with addition of zinc acetate $Zn(CH_3COO)_2{\cdot}2H_2O$ in the quantity of 0.076 mol.% with the final annealing at 500 ± 5 °C for 60 min.

For the experimental study, the titanium dioxide sols were also prepared: base sol TiO_2. Titanium dioxide sol were produced by hydrolysis of tetrabutoxytitanium (TBT): $(C_3H_8O)4Ti$ (mass fraction of main substance 98.9%, special purity; TU 2637-059-44493179-04). The solvent used was 96% solution of ethyl alcohol (GOST 18300-87). As the reaction inhibitor, acetic acid CH_3COOH was used (mass fraction of main substance 99.8%, chemically pure; GOST 61-75). Ratio of mixture components by mass of $TBT : H_2O : C_2H_5OH : CH_3COOH = 0.46 : 1.76 : 14.78 : 0.09$. In a reaction cup ethanol and acetic acid were mixed for 2−3 min, then TBT, 97% was added (SigmaAldrich244112).

Kinematic viscosity of synthesized sols was measured for 3−5 days using a capillary viscosimeter ($d_{cap} = 0.86$ mm) (GOST 33-2000) at temperature $T = 20 \pm 1$ °C. The produced sols were applied on the plates of silicate glass of crown group of *K*8 ($n = 1.52$) type and leucosapphire plates ($n = 1.8$) by method of pulling from the solution at temperature of 20 ± 1 °C. Coatings were applied after maturing of sols preventing gel formation in solutions. Glass substrates were cleaned by boiling in the hydrogen peroxide solution. Speed of extraction from solution was selected in the range of 100−180 mm/min.

The general view of the two-side antireflection coating applied on the glass substrate is given in Fig. 1.

The method to apply a three-layer coating consisted of three stages. At each stage of application, thermal annealing of the coating was carried out at 500 °C. At the first stage a hybrid coating based on SiO_2@TiO_2 was applied on the glass. At the following stage TiO_2 coating was applied. The final stage of the developed method was application of SiO_2 coating. The general view of the two-side three-layer antireflection coating on the glass substrate (SiO_2@TiO_2)−TiO_2−SiO_2 was not given.

The roughness of the produced coatings was studied using a microscope of a probe nanolaboratory *NT-MDTNtegraSpectra*, in semi-contact mode. Probes of NSG10 series made by NTMDT were used. To determine the thickness of the film and roughness of the coatings, software was used to analyze the data of scanning probe microscopy *Gwyddion.*

Spectral optical characteristics were modeled by the analytical method for evaluation of the input impedance of the multilayer structure using Fresnel formulae. It is known that for electromagnetic wave (EMW) along axis z admittance $A(z, k) = H_t(z, k)/E_t(z, k)$ and impedance $Z(z, k)$ of the electromagnetic field are defined as $Z(z, k) = 1/A(z, k) = E_t(z, k)/H_t(z, k)$. To minimize the reflection of the electromagnetic radiation from the interface between the coating and the air, it is necessary to most fully

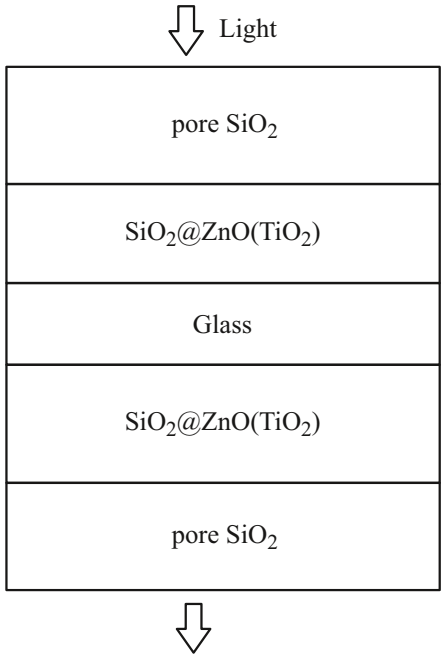

Figure 1. General view of two-side antireflection coating on glass substrate.

provide for the broadband optical agreement by impedance of the substrate with the coating and the environment. It is known that the impedance of medium Z_m is determined by the inverse value of the module of its complex refractive index as $Z_m = \frac{Z_0}{|\hat{n}_m|} = \frac{Z_0}{\sqrt{n^0+k^2}}$, where $Z_0 = 377\,\Omega$, impedance of free space; $\hat{n}_m = n - jk$ — complex refractive index of the medium, n — refractive index, k — absorption index or extinction coefficient. Essentially, ARC is a transformer of environment and substrate impedances. For transparent and absorbing substrates, ARCs must provide for the optical transparency that does not depend on the angle of light incidence. Ideal elucidation occurs upon compliance with the condition $Z_m = Z_0$ or $\sqrt{n^2 + k^2} = 1$.

Each separate layer was considered as a section of a long line with its complex wave impedance $\hat{Z}_{0j} = Z_a/\hat{n}_j$, where Z_a — wave impedance of the environment (for air $Z_a = 377\,\Omega$), $\hat{n}_j = n_j - ik_j$ — complex refractive index of jth layer. The essence of the method consists in finding the input impedance of $\hat{Z}_{in}$ multilayer coating on a glass substrate. Knowing it and applying the Fresnel formulae, it is easy to obtain the ratio to estimate the amplitude reflection coefficient $\hat{r}$ and transmittance coefficient $\hat{t}$. For transverse polarization of light the ratios for $\hat{r}_s$ and $\hat{t}_c$ and for longitudinal $\hat{r}_p$ and $\hat{t}_p$ have the following appearance [9]:

$$\hat{r}_s = \frac{\hat{Z}_m \cos\theta - Z_{in}\cos\gamma}{\hat{Z}_m \cos\theta + Z_{in}\cos\gamma}, \tag{1}$$

$$\hat{t}_s = \frac{2\hat{A}_{in}\cos\theta}{\hat{Z}_m \cos\theta + Z_{in}\cos\gamma}, \tag{2}$$

$$\hat{r}_p = \frac{\hat{Z}_{in}\cos\theta - Z_m\cos\gamma}{\hat{Z}_{in}\cos\theta + Z_m\cos\gamma}, \tag{3}$$

$$\hat{t}_p = \frac{2\hat{A}_{in}\cos\theta}{\hat{Z}_{in}\cos\theta + Z_m\cos\gamma}, \tag{4}$$

where θ — angle of incidence of optical wave at the input boundary of ARC, γ — angle of light refraction. For further consideration, it is convenient to present the amplitude reflection coefficients for the light polarized in different planes in the unified form:

$$\hat{r}_{s,p} = \frac{\hat{n}_1 - \hat{n}_2}{\hat{n}_1 + \hat{n}_2},$$

where

$$\hat{n}_i = \begin{cases} n_i\cos\theta_i \\ \frac{\cos\theta_i}{n_i} \end{cases}$$

for p- and s-components respectively.

In contrast to the widely known matrix method of light transmittance modeling in multilayer film structures, this paper proposes a new modification of the impedance method to calculate [15,16] spectral reflection and transmittance of light in such structures. The impedance method is widely used in the theory of long lines and waveguide structures. Comparison of the calculation results using two methods demonstrated their high degree of match. However, the impedance method of calculation, in our opinion, has a simpler form.

The input impedance of jth layer of ARC $\hat{Z}^j_{in}$ with wave resistance $\hat{Z}^j_0$ and resistance of the $\hat{Z}^{j-1}_0$ layer load is recorded in the following form:

$$\hat{Z}^j_{in} = A_j + iB_j = \hat{Z}^j_0 \frac{\hat{Z}^{j-1}_0 + i\hat{Z}^j_0 \tan\varphi_j}{\hat{Z}^j_0 + i\hat{Z}^{j-1}_0 \tan\varphi_j}, \tag{5}$$

where $\varphi_j = \left(\frac{2\pi}{\lambda}\right) n_j d_j$ — phase thickness of jth layer [9]. For jth layer, the load is input impedances of all prior layers together with the substrate. The calculations are carried out from the first layer loaded onto the substrate.

The module of wave resistance of jth layer of ARC Z^j_0 may be recorded in the following form

$$Z^j_0 = \frac{Z_0}{\sqrt{n_j^2 + k_j^2}},$$

and real and imaginary parts of wave resistance of jth layer of ARC in ratio (5) will be recorded by us in the following form

$$A_j = Z_0 \frac{n_j}{n_j^2 + k_j^2} \quad \text{and} \quad B_j = Z_0 \frac{k_j}{n_j^2 + k_j^2}. \tag{6}$$

Spectral expressions for the real and imaginary parts of input resistance of jth layer from ratio (5) will be recorded by us as

$$A_j(\lambda) = A_{j-1}(\lambda)\left[\frac{1 + \tan^2\varphi_{j-1}(\lambda)}{E^2_{j-1}(\lambda) + F^2_{j-1}(\lambda)}\right],$$

$$B_j(\lambda) = \frac{B_{j-1}(\lambda)(1-\tan^2\varphi_{j-1}(\lambda)) - \tan\varphi_{j-1}(\lambda) \times[(A_{j-1}^2(\lambda)+B_{j-1}^2(\lambda))(\frac{1}{Z_0^{j-1}}) - Z_0^{j-1}]}{E_{j-1}^2(\lambda)+F_{j-1}^2(\lambda)}, \quad (7)$$

where

$$E_{j-1}(\lambda) = 1 - B_{j-1}(\lambda)\left(\frac{1}{Z_0^j}\right)\tan\varphi_{j-1}(\lambda)$$

and

$$F_{j-1}(\lambda) = A_{j-1}(\lambda)\left(\frac{1}{Z_0^j}\right)\tan\varphi_{j-1}(\lambda).$$

For the substrate the real and imaginary parts of wave resistance according to (6) have the following form

$$A_s = Z_0\frac{n_s}{n_s^2+k_s^2} \quad \text{and} \quad B_s = Z_0\frac{k_s}{n_s^2+k_s^2},$$

where n_s and k_s — respectively, the refractive index and the absorption index of the substrate.

Using ratios (8), it is easy to record the real and imaginary parts of input resistance for the first layer applied on the substrate as

$$A_1(\lambda) = A_s(\lambda)\left[\frac{1+\tan^2\varphi_s(\lambda)}{E_s^2(\lambda)+F_s^2(\lambda)}\right],$$

$$B_1(\lambda) = \frac{B_s(\lambda)(1-\tan^2\varphi_s(\lambda)) - \tan\varphi_s(\lambda)[(A_s^2(\lambda)+B_s^2(\lambda))(\frac{1}{Z_0^s}) - Z_0^s]}{E_s^2(\lambda)+F_s^2(\lambda)}, \quad (8)$$

where

$$E_s(\lambda) = 1 - B_s(\lambda)\left(\frac{1}{Z_0^s}\right)\tan\varphi_s(\lambda),$$

$$F_s(\lambda) = A_s(\lambda)\left(\frac{1}{Z_0^s}\right)\tan\varphi_s(\lambda),$$

$$Z_0^s = \frac{Z_0}{\sqrt{n_s^2+k_s^2}},$$

$$\varphi_s = \left(\frac{2\pi}{\lambda}\right)n_s d_s.$$

Here d_s — substrate thickness.

For a single-layer ARC the input impedance, according to (5) and (8), will be recorded as

$$\hat{Z}_{in} = A_{in} + iB_{in},$$

where

$$A_{in}(\lambda) = A_1(\lambda)\left[\frac{1+\tan^2\varphi_1(\lambda)}{E_1^2(\lambda)+F_1^2(\lambda)}\right],$$

$$B_{in}(\lambda) = \frac{B_1(\lambda)(1-\tan^2\varphi_1(\lambda)) - \tan\varphi_1(\lambda)[(A_1^2(\lambda)+B_1^2(\lambda))(\frac{1}{Z_0^1}) - Z_0^1]}{E_1^2(\lambda)+F_1^2(\lambda)}, \quad (9)$$

$$E_1(\lambda) = 1 - B_1(\lambda)\left(\frac{1}{Z_0^1}\right)\tan\varphi_1(\lambda),$$

$$F_1(\lambda) = A_1(\lambda)\left(\frac{1}{Z_0^1}\right)\tan\varphi_1(\lambda),$$

$$Z_0^1 = \frac{Z_0}{\sqrt{n_1^2+k_1^2}},$$

$$\varphi_1 = \left(\frac{2\pi}{\lambda}\right)n_1 d_1.$$

Here d_1 — layer thickness.

Using Fresnel formulae (1)–(4), we will record the amplitude reflection and transmittance coefficients for EMW for s- and p-polarization as

$$\operatorname{Re} r_s(\lambda) = \frac{[A_{in}^2(\lambda)+B_{in}^2(\lambda)]\cos^2\theta - Z_0^2\cos^2\gamma}{[A_{in}(\lambda)\cos\theta + Z_0\cos\gamma]^2 + [B_{in}(\lambda)\cos\theta]^2},$$

$$\operatorname{Im} r_s(\lambda) = \frac{2B_{in}(\lambda)Z_0\cos\theta\cos\gamma}{[A_{in}(\lambda)\cos\theta + Z_0\cos\gamma]^2 + [B_{in}(\lambda)\cos\theta]^2},$$

$$\operatorname{Re} r_t(\lambda) = \frac{Z_0^2\cos^2\theta - [A_{in}^2(\lambda)+B_{in}^2(\lambda)]\cos^2\gamma}{[A_{in}(\lambda)\cos\gamma + Z_0\cos\theta]^2 + [B_{in}(\lambda)\cos\gamma]^2},$$

$$\operatorname{Im} r_t(\lambda) = \frac{2B_{in}(\lambda)Z_0\cos\theta\cos\gamma}{[A_{in}(\lambda)\cos\gamma + Z_0\cos\theta]^2 + [B_{in}(\lambda)\cos\gamma]^2}.$$

The energy module of the reflection coefficient has the following appearance

$$R_{s,t}(\lambda) = |r_{s,t}(\lambda)|^2 = \sqrt{\operatorname{Re} r_{s,t}(\lambda)^2 + \operatorname{Im} r_{s,t}(\lambda)^2}.$$

For nonpolarized light

$$R(\lambda) = \left(\frac{R_s(\lambda)+R_t(\lambda)}{2}\right)a_1, \quad (10)$$

where coefficient $a_1 = 1$ for the single-layer coating on the substrate and $a_1 = 2$ for the two-sided one. For example, the reflection coefficient of the glass plate with two free boundaries is equal to 8%.

Based on the energy balance, the transmittance coefficient may be recorded as $T(\lambda) = 1 - R(\lambda) - A(\lambda)$, where $A(\lambda)$ — coefficient of losses in ARC.

If there are no losses, or losses are insignificant in ARC the transmittance coefficient may be recorded as $T(\lambda) = 1 - R(\lambda)$.

Technology of sol-gel application of ARC makes it possible to create composite nanocoatings on any substrates with controlled parameters for optical thicknesses of coatings (refractive index and geometric thickness). In this paper the following basic materials were selected: a silicate glass substrate of crown group $K8$ ($n = 1.52$) and leucosapphire plate ($n = 1.8$), silicon dioxide (SiO_2, $n = 1.45$), titanium dioxide (TiO_2, $n = 2.6$) and zinc oxide (ZnO, $n = 2.0$). To calculate the effective values of refractive index, methods were used on the basis of Lichtenegger and Bruggeman equations described in paper [12]. The top later was porous

silicon dioxide with refractive index within 1.45 - 1.35. The bottom layer loaded onto the glass substrate was a matrix composite nanomaterial SiO_2@ZnO with mass concentration in the range of (1−10) mas% or volume fraction p of ZnO inclusion into matrix SiO_2 ($p = 0.005-0.05$). The refractive index of the composite nanocoating SiO_2@ZnO was in the range of (1.45−1.48). Another matrix composite nanomaterial was SiO@TiO_2. For mass concentration (1−10) mas% or volume fraction of inclusion of TiO_2 into matrix SiO_2 ($p = 0.0063-0.065$) the refractive index of the composite nanocoating of SiO_2@TiO_2 was in the range of (1.45−1.52).

The thickness of coatings was determined after thermal treatment by contact method in profilometer Veeco Dektac 150 (Veeco Instruments Inc., USA).

Optical spectral measurements of transmittance of glass plates with applied coatings were carried out using the diagram described below. The light beam from Ocean OpticsDH-2000-BAL lamp via a light guide (optic fiber Ocean OpticsP-100-2-UV-VIS) and collimator falls at the specified angle at the sample. The sample was located on the site of goniometer Standa 068979. The reflected light beam via collimator OceanOptics 74 DA and optic fiber entered the input of spectrometer OceanOpticsQE 65000.

Results and discussion

To determine the fundamental dependences of coating properties on the parameters of their application, studies of rheological properties of sols were conducted depending on the duration of their maturing. The sols produced in the experiment were studied for the stability of gel formation. Over time, the change in the kinetic viscosity was recorded using viscosimeter VPZh-1. The obtained data of kinetic viscosity change in sols of silicon dioxide, titanium dioxide and their compositions are presented respectively in Fig. 2.

As it follows from the given dependences in Fig. 2, sols of silicon dioxide and titanium dioxide (curves *1* and *2*) are stabilized on day 6. Whereas in hybrid (mixed) sol of titanium and silicon oxides (curve *3*) for two days the hydrolysis process is happening, and on day 4 the gel is formed with sedimentation.

With the selected viscosity of sol, the thickness of the produced coating depends on the speed of substrate pulling from sol. As the speed of coating pulling from the solution increases, its thickness increases.

Tests of the glass samples with the applied ARC for moisture resistance and abrasive resistance according to the requirements of the European standard EN 1096-2 „Glass in building — Coated glass“ found that moisture resistance and abrasive resistance corresponding to class *A* are possessed by the coating that underwent isothermal soaking at temperature of $500 \pm 5\,^{\circ}$C. The change in the optical transmittance coefficient of the sample before and after tests at $\lambda = 550$ and 900 nm was no more than 0.2% for both wavelengths. Consequently, glass with the

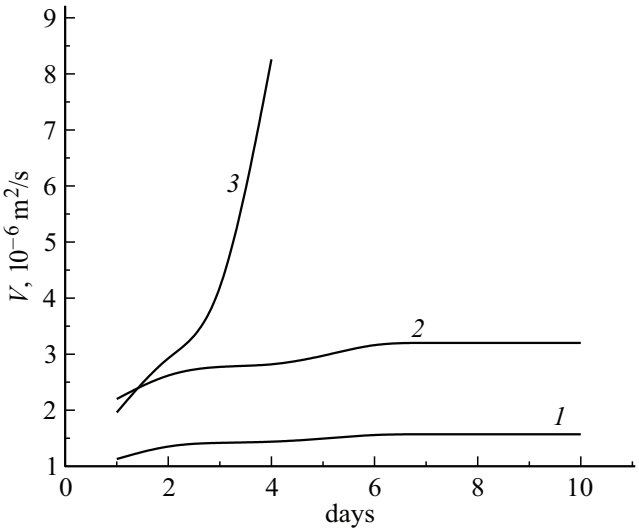

Figure 2. Change of kinematic viscosity of sol of silicon, titanium dioxides and composite of silicon dioxide with addition of titanium dioxide over time. Curve *1* — SiO_2, *2* — TiO_2, *3* — SiO_2@TiO_2.

deposited ARC that has undergone isothermal holding in a furnace at a temperature of $500 \pm 5\,^{\circ}$C for 15 ± 1 min can be used for outdoor applications. After the adhesion tests, the optical properties of the coatings were re-examined.

An important advantage of composite nanomaterials of multilayer coatings is the ability to control the effective refractive index of the entire structure. This paper used porous nanomaterials, silicon and titanium dioxides, and two types of matrix nanomaterials — with matrix from SiO_2 and filler from TiO_2 and matrix from TiO_2 and filler from SiO_2.

The values of the effective refractive index n_{ef} were calculated using the Lichtenegger formula [17]: $n_{ef} = f_p n_p + (1 - f_w n_m)$, where $f_p = \frac{V_p}{V_m}$ — volume fraction of the filler, $f_w = \frac{m_p}{m_m}$ — mass fraction of the filler, n_p and n_m — refractive indices of the filler and matrix, accordingly. The volume and mass fractions are related with the following ratio:

$$f_p = \frac{f_w}{f_w + (1 - f_w)\frac{\rho_p}{\rho_m}},$$

where ρ_p, ρ_m — densities of the filler and matrix material accordingly (g/cm^3).

Fig. 3 shows the calculated dependences of the effective refractive index of a composite nanocoating based on silicon and titanium dioxides on the volume fraction of filler. For composite nanomaterials based on silicon dioxide and zinc oxide, the values of the effective refractive index are given in detail in [12].

The range of variation of the effective refractive index of the composite material largely depends on the ratio of the matrix and filler refractive indices. Fig. 4 shows the calculated dependences of the effective refractive index of composites based on silicon dioxide and different fillers. The calculations used the following values of refractive

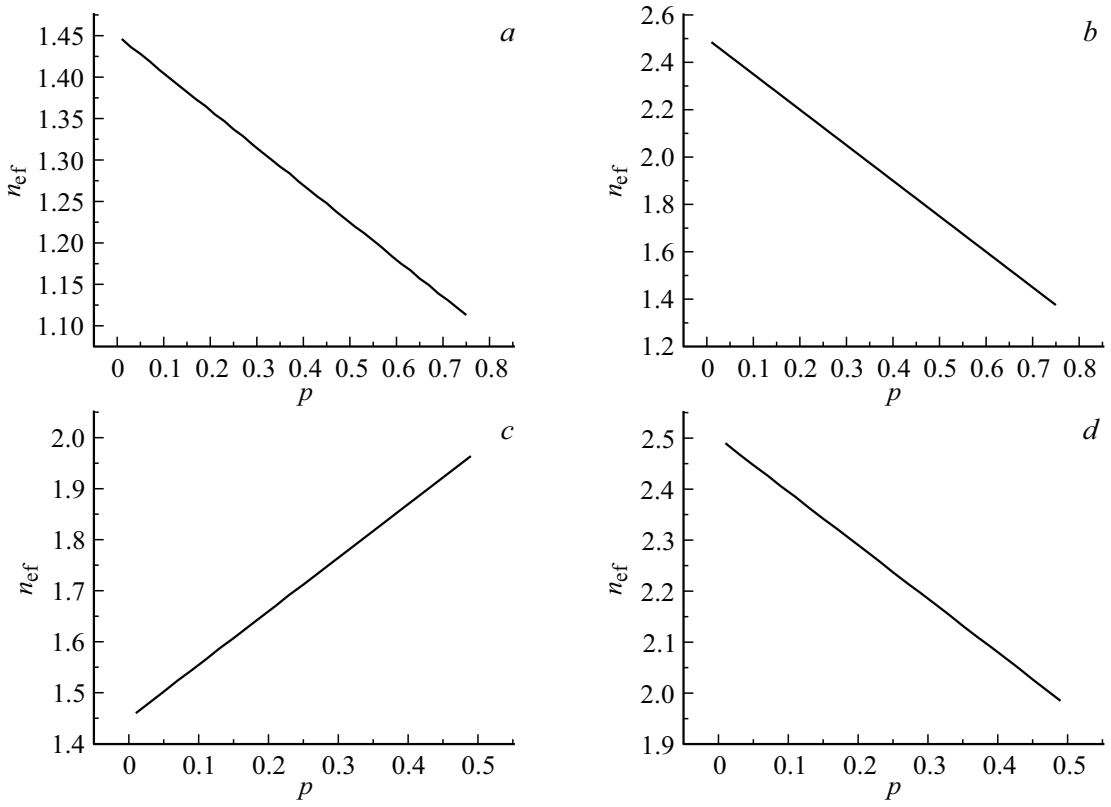

Figure 3. Dependences of effective refractive index of composite nanocoating on volume fraction of filler: (*a*) porous silicon dioxide with air filling ($n_m = 1.45$; $n_f = 1$); (*b*) tubular titanium dioxide with air filling ($n_m = 2.5$; $n_f = 1$); (*c*) silicon dioxide with a filler from titanium dioxide ($n_m = 1.45$; $n_f = 2.5$); (*d*) titanium dioxide with a filler from silicon dioxide ($n_m = 2.5$; $n_f = 1.45$).

indices: matrix from SiO_2 ($\rho_m = 2.648\,g/cm^3$, $n_m = 1.45$), filler from ZnO ($\rho_f = 5.61\,g/cm^3$, $n_f = 2.03$), filler from TiO_2 ($\rho_f = 4.23\,g/cm^3$, $n_f = 2.65$). From the given dependences, it follows that the use of titanium dioxide filler significantly increases the range of variation of the effective refractive index values of the composite coating.

Single-layer coatings based on the composite nanomaterial SiO_2@ZnO were studied in detail in our paper [12]. The advantages of using two-layer coatings from the same material are shown in Fig. 5, which shows the spectral difference of the measured optical transmittance of samples with a single-layer SiO_2@ZnO coating (curve *1*) and a two-layer SiO_2-SiO_2@ZnO coating (curve *2*) on a glass substrate and the glass substrate itself.

From the given spectral dependences, it follows that the optical transmittance of the two-layer structure is generally higher in the visible region of the optical spectrum. This is more pronounced in the short-wavelength part of the spectrum. The single-layer ARC structure was fabricated at a drawing speed of 160 mm/min from the composite nanomaterial SiO_2@ZnO, where SiO_2 was chosen as the matrix and 10 mas]% ZnO, as the filler. The two-layer ARC structure was fabricated at a drawing speed of 138 mm/min from the composite nanomaterial, where SiO_2@ZnO (10 mas%) was chosen as the bottom layer on the glass substrate, and the top layer material was made

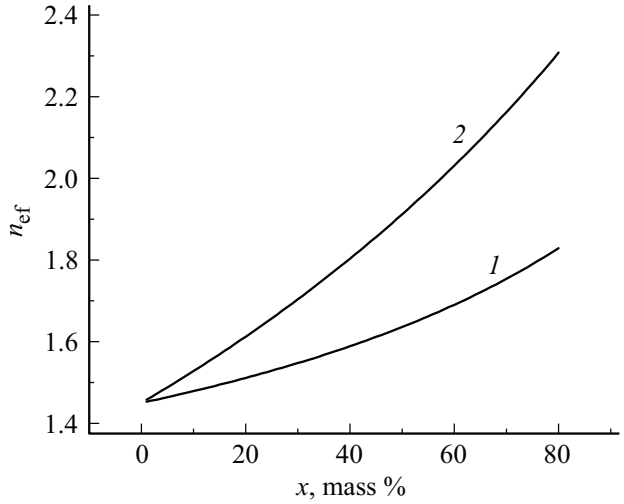

Figure 4. Dependences of effective refractive index of composites based on silicon dioxide SiO_2 on mass concentration of fillers: ZnO (*1*), TiO_2 (*2*).

of porous SiO_2 (22 pore%). Individual measurements of the refractive index of each layer demonstrated that the refractive index of the porous SiO_2 is 1.35, and the refractive index of the bottom layer SiO_2@ZnO (10 mas%) is 1.47.

Apart from composite nanocoatings from SiO_2@ZnO, the paper studied ARCs based on SiO_2@TiO_2. Single-layer, two-layer, and three-layer composite nanocoatings were fabricated. The spectral reflection characteristics were measured and the effective refractive index of such coatings was estimated. Fig. 6 shows the spectral dependences of optical reflection and the effective refractive index of SiO_2-SiO_2@TiO_2 coatings on glass substrates. The single-layer coating consisted of porous SiO_2 (pore 22%) with a thickness of 117 nm and a refractive index of 1.35. In the two-layer coating, the bottom layer on the substrate was made of nanocomposite SiO_2@TiO_2 (22 mas%) with a thickness of 185 nm and a refractive index of 1.7, the top layer was porous SiO_2 (pore 22%) with a coating thickness of 117 nm and a refractive index of 1.35. The three-layer coating consisted of the following layers: bottom layer on the substrate — porous SiO_2 (pore 22%) with a thickness of 117 nm and refractive index of 1.35; middle layer — nanocomposite SiO_2@TiO_2 (22 mas%) with a thickness of 185 nm and refractive index 1.7; top layer — porous SiO_2 (pore 22%) with a thickness of 117 nm and refractive index 1.35. Based on the measured energy spectra of reflection, it is easy to estimate the spectral values of the effective refractive index of the composite coating. In the assumption of no optical losses in the structure let us record the law of conservation of energy as $R(\lambda) + T(\lambda) = 1$. Spectral reflection is related to the effective refractive index of the coating as $R(\lambda) = \left(\frac{1-n_{ef}(\lambda)}{1+n_{ef}(\lambda)}\right)^2$. Then the spectral effective refractive index may be estimated as $n_{ef}(\lambda) = \frac{1+R(\lambda)+\sqrt{R(\lambda)}}{1-R(\lambda)}$ or $n_{ef}(\lambda) = \frac{1}{T(\lambda)} + \sqrt{\left(\frac{1}{T(\lambda)^2}\right) - 1}$.

From the dependences given in Fig. 6 it follows that the two-layer coating provides for the lowest reflection in the entire spectral range from 400 to 900 nm. It is reasonable to use the three-layer coating, when narrow-band elucidation is required with significant offset of spectral areas of the minimum reflection. The paper [9] considers in detail the conditions of the minimum optical reflection of the structures based on two-layer ARCs. To zero the energy reflection coefficient $R = 0$, it is necessary to meet the following condition:

$$\begin{cases} (n_0 - n_m)\cos\varphi_1\cos\varphi_2 + \left(\frac{n_0 n_2}{n_1} - \frac{n_m n_1}{n_2}\right)\sin\varphi_1\sin\varphi_2 = 0, \\ \left(\frac{n_0 n_m}{n_1} - n_1\right)\sin\varphi_1\cos\varphi_2 + \left(\frac{n_0 n_m}{n_2} - n_2\right)\cos\varphi_1\sin\varphi_2 = 0, \end{cases}$$

where n_0, n_1, n_2, n_m — refractive indices of the environment ($n_0 = 1$), top layer (n_1), bottom layer (n_2) and substrate (n_m). Phase thicknesses of the top and bottom layers will be designated accordingly as $\varphi_1 = 2\pi n_1 d_1/\lambda$ and $\varphi_2 = 2\pi n_2 d_2/\lambda$. Assuming n_1 and n_2 to be fixed values, we will get the system of two equations relative to the phase thicknesses of the layers. After transformation, the condition must be satisfied: $\tan^2\varphi_1 > 0$ and $\tan^2\varphi_2 > 0$. If we designate the factors as $A = (n_0 n_m - n_2^2)$, $B = (n_0 n_m - n_1^2)$, $C = (n_0 n_2^2 - n_1^2 n_m)$, then for positive values of the squared tangents φ_1 and φ_2 certain values of the refractive indices must be chosen. These values must satisfy the following inequalities [9]:

$$\begin{cases} (n_0 n_m) - n_2^2 > 0 \\ (n_0 n_m) - n_1^2 > 0 \\ n_0 n_2^2 - n_m n_1^2 > 0 \end{cases} \quad (11)$$

$$\begin{cases} (n_0 n_m) - n_1^2 < 0 \\ n_2^2 - n_0 n_m > 0 \\ n_0 n_2^2 - n_m n_1^2 < 0 \end{cases} \quad (12)$$

$$\begin{cases} (n_0 n_m) - n_1^2 > 0 \\ n_2^2 - n_0 n_m > 0 \\ n_0 n_2^2 - n_m n_1^2 < 0 \end{cases} \quad (13)$$

$$\begin{cases} (n_0 n_m) - n_1^2 < 0 \\ n_2^2 - n_0 n_m > 0 \\ n_0 n_2^2 - n_m n_1^2 > 0 \end{cases} \quad (14)$$

If we require that the energy reflection coefficient be zero at a wavelength $\lambda = \lambda_0$, then it is easy to determine the optical thicknesses of the layers at which the reflection coefficient is zero: $n_1 d_1 = (\lambda_0/2\pi)\,\mathrm{atan}\,(A)$, $n_2 d_2 = -(\lambda_0/2\pi)\,\mathrm{atan}\,(B)$. To satisfy this condition, the inequalities for the optical thicknesses of the layers must be met: $n_1 d_1 < (\lambda_0/4)$ and $n_2 d_2 > (\lambda_0/4)$.

For a composite two-layer nanocoating SiO_2–SiO_2@TiO_2(TiO_2@SiO_2), by choosing the matrix and filler material, it is possible to vary the refractive index of the bottom layer loaded onto the glass substrate over a wide range from 1.7 to 2.3. The geometric layer thickness varied from 130 to 190 nm due to different drawing speeds

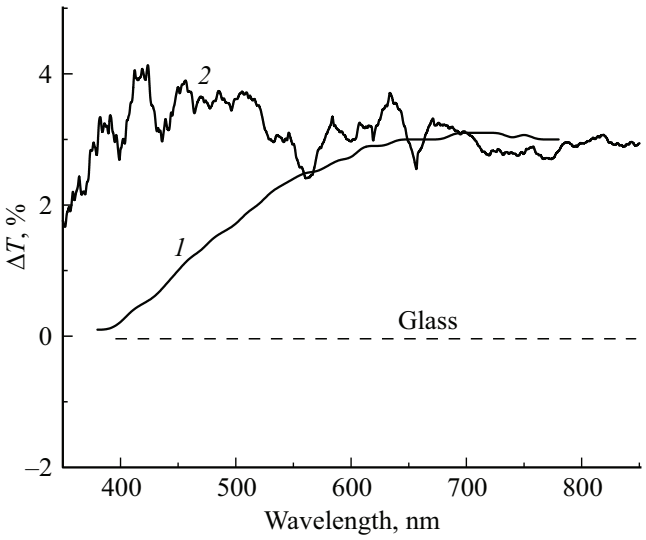

Figure 5. Difference of measured spectra of optical transmittance of samples with a single-layer SiO_2@ZnO (*1*) coating and a two-layer SiO_2–SiO_2@ZnO (*2*) coating on a glass substrate and of the glass substrate itself.

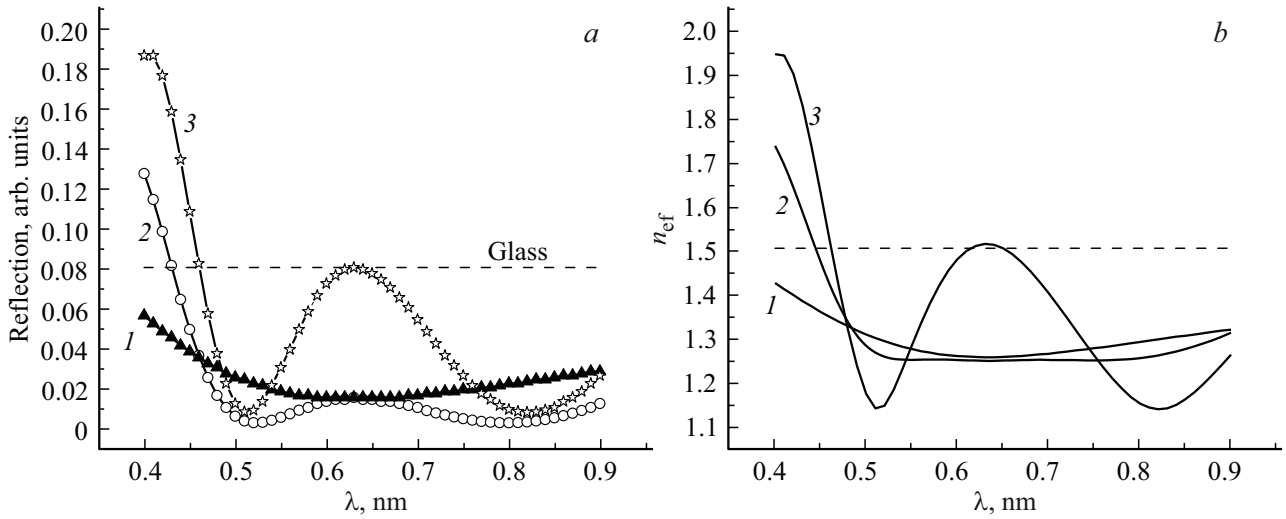

Figure 6. Measured spectral dependences of optical reflection and estimated data of the effective refractive index of one-, two- and three-layer coatings SiO_2 and $SiO_2@TiO_2$ on the glass substrates: (*a*) optical reflection, (*b*) effective refractive index (*1* — one layer SiO_2, *2* — two layers $SiO_2-SiO_2@TiO_2$, *3* — three layers $SiO_2-SiO_2@TiO_2-SiO_2$).

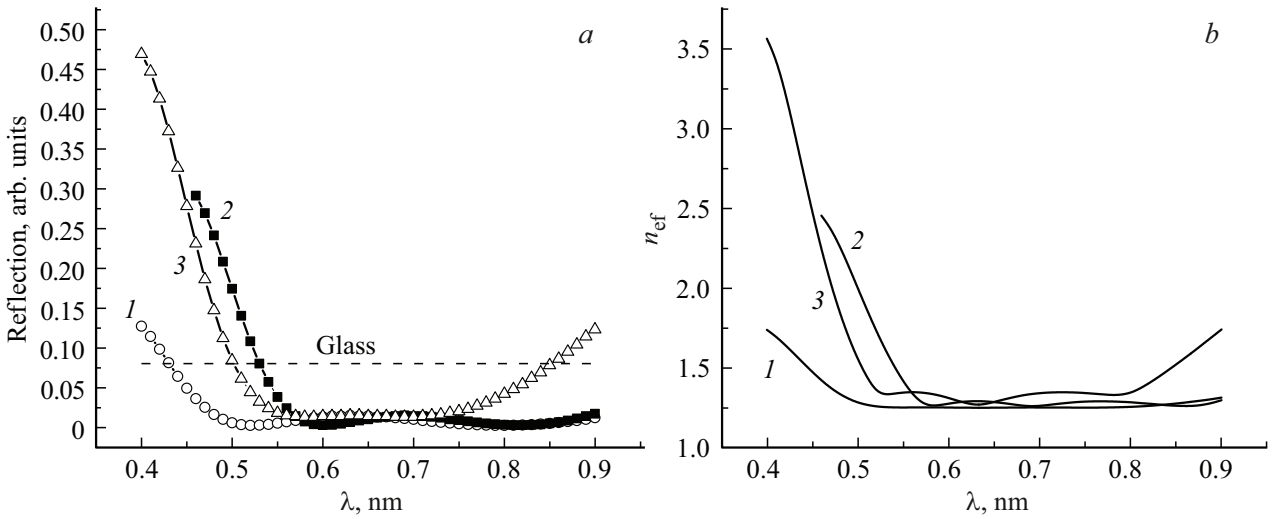

Figure 7. Estimated spectral dependences of optical reflection and effective refractive index of two-layer coatings $SiO_2-SiO_2@TiO_2$ on glass substrates and variable value of refractive index of the layer on the substrate (n_{bot}): (*a*) optical reflection, (*b*) effective refractive index (*1* — $n_{bot} = 1.7$; *2* — $n_{bot} = 2.0$; *3* — $n_{bot} = 2.3$).

and solution viscosities. The top layer of porous silicon had constant values of refractive index equal to 1.35 and thickness of 117 nm.

Fig. 7 shows the estimated spectral dependences of optical reflection and data for the effective refractive index of two-layer $SiO_2-SiO_2@TiO_2$ coatings on glass substrates with different values of the refractive index of the layer on the substrate (n_{bot}). From the given dependences, it follows that an increase in the refractive index of the bottom layer narrows the optical wavelength range of minimum reflection.

Since in our paper we selected the following refractive indices: $n_m = 1.52$ and $n_m = 1.8$, (pore SiO_2), ($SiO_2@ZnO$), ($SiO_2@TiO_2$), then depending on the substrate material choice, the condition of minimum reflection is satisfied for inequalities (12) and (14). Inequality (14) is satisfied for the substrate from crown silicate glass ($n_m = 1.52$), and inequality (12) is satisfied for the glass substrate from heavy flint or leucosapphire ($n_m = 1.8$).

Fig. 8 shows the estimated spectral difference of optical reflection of samples with a two-layer $SiO_2-SiO_2@TiO_2$ coating on different glass substrates. The condition for zeroing the energy reflection coefficient of the coating $R = 0$ is satisfied when $(R_g - R)/R_g \to 1$, where R_g is the energy reflection coefficient of the bare glass surface. For the coating on silicate glass, the antireflection ability turned out to be higher than on glass with an increased refractive index.

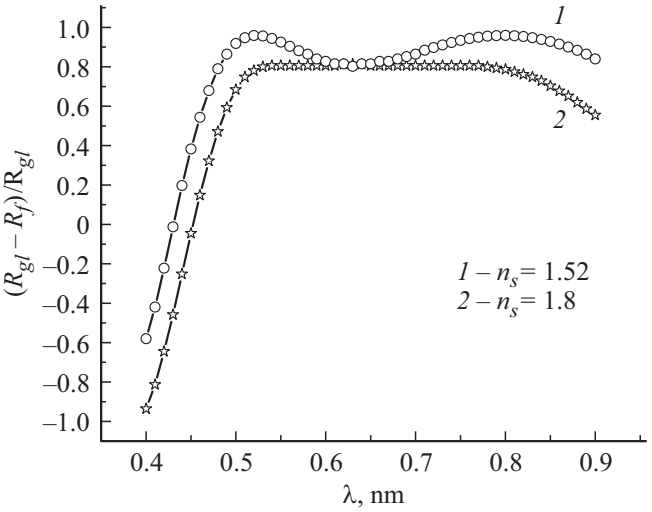

Figure 8. Estimated spectral difference of optical reflection of samples with a two-layer $SiO_2-SiO_2@TiO_2$ coating on different glass substrates: *1* — substrate from the crown silicate glass ($n_s = 1.52$), a layer on the substrate ($n_{bot} = 1.7$, $d_{bot} = 185$ nm), the top layer ($n_{top} = 1.35$, $d_{bot} = 115$ nm); *2* — the substrate from heavy flint glass ($n_s = 1.8$), a layer on the substrate ($n_{bot} = 2.2$, $d_{bot} = 144$ nm), the top layer ($n_{top} = 1.45$, $d_{bot} = 109$ nm).

Thus, studies of the antireflection ability of multilayer composite nanocoatings have shown that the optimal coating variant is two-layer coatings, which possess high antireflective properties and the potential for application to glasses with different refractive indices.

Conclusion

Based on sol-gel technological methods, multilayer antireflective coatings have been developed for crown-type glass *K*8 ($n = 1.52$) and leucosapphire plates ($n = 1.8$). Liquid coatings were applied to glass substrates by the pulling method at a speed in the range of 100 to 180 mm/min. The thickness of the deposited coatings was measured for glasses annealed at 500 °C. The thickness of the SiO_2 layer ranged from 100.5 to 120.5 nm. The thicknesses of the composite layers were: $SiO_2@ZnO$ 100 ± 10 nm, $SiO_2@TiO_2$ from 140 ± 5 to 185 ± 5 nm. Based on the comparison of the transmittance spectra of single-layer $SiO_2@ZnO$ and two-layer coatings $SiO_2-SiO_2@ZnO$ it was shown that the two-layer coatings are more transparent in the violet area of the spectrum. Based on measurements of the reflection spectra of single-layer (SiO_2), two-layer ($SiO_2-SiO_2@TiO_2$) and three-layer ($SiO_2-SiO_2@TiO_2-SiO_2$) coatings, it can be stated that these coatings correspond to the current state of the art in the development of multilayer coatings, as presented, for example, in the review [18]. It should be noted that two-layer mesoporous composite coatings with different compositions best demonstrate the antireflective ability of glasses with medium (1.52) and high (1.8) refractive indices.

Funding

This work was supported by the Ministry of Science and Higher Education of the Russian Federation under the state assignment of the V.A. Kotelnikov Institute of Radio Engineering and Electronics of the Russian Academy of Sciences (FFWZ-2025-0001).

Conflict of interest

The authors declare that they have no conflict of interest.

References

[1] H. Liu, P. Wang, Q. Fan, J. Luo, P. Xiao, B. Jiang. Coatings, **12**, 435 (2022). DOI: 10.3390/coatings12040435
[2] W. Zhao, H. Jia, J. Qu et al. J. Sol-Gel Science and Technology, **107** (1), 105–121 (2023). DOI: 10.1007/s10971-021-05719-3
[3] G.J. Hou, I. García, I. Rey-Stolle. Solar Energy, **217**, 29–39 (2021). DOI: 10.1016/j.solener.2021.01.060
[4] F. Hassan-Aghaei, M.M. Mohebi. Optical Materials, **135**, 113246 (2023). DOI: 10.1016/j.optmat.2022.113246
[5] S. Kumar, M. Malik, R. Purohitc. Materials Today: Proc., **4**, 350–357 (2017). DOI: 10.1016/j.matpr.2017.01.032
[6] A.A. Tokranov, E.O. Tokranova, R.V. Shafigulin, A.V. Bulanova. Surface Physicochemistry and Material Protection, **60** (4), 379–388 (2024).
[7] B.J. Scott, G. Wirnsberger, G.D. Stucky. Chem. Mater., **13** (10), 3140–3150 (2001). DOI: 10.1021/cm0110730
[8] Di Liua, Jiawei Wan, Hong Wang, Gangsheng Panga, Zhiyong Tang. Inorganic Chemistry Communications, **102**, 203–209 (2019). DOI: 10.1016/j.inoche.2019.02.031
[9] E.S. Putilin. Optical Coatings. Tutorial. (SPbSUITMO, St. Petersburg, 2010.
[10] X. Sun, K. Hu, J. Tu, K. Chen. Surfaces and Interfaces, **24**, 101135 (2021). DOI: 10.1016/j.surfin.2021.101135
[11] J. Qu, H. Jia, W. Wang, Y. Wang, S. Zhu. Silicon, **15**, 4959–4966 (2023). DOI: 10.1007/s12633-023-02411-9
[12] N.A. Malofeeva, I.N. Mikhailov, S.S. Volchkov, M.Yu. Vasilkov, I.D. Kosobudskii, N.M. Ushakov. Bulletin of Saratov University. New series. Series: Physics, **24** (3), 271–280 (2024). DOI: 10.18500/1817-3020-2024-24-3-271-280.
[13] L. Yao, J. He. J. Mater. Chem. A, **2**, 6994–7003 (2014). DOI: 10.1039/C3TA15363K
[14] L. Ye, X. Ge, X. Wang, Z. Hui, Y. Zhang. Ceramics International. Part A, **45** (7), 8504–8509 (2019). DOI: 10.1016/j.ceramint.2019.01.162
[15] R. Pregla. In: J. Jahns, K.H. Brenner (eds). Microoptics. Springer Series in Optical Sciences, **97** (Springer, N.Y., 2004). DOI: 10.1007/978-0-387-34725-7_5
[16] S. Chialina, M. Cicuttin, L. Codecasa, R. Specogna, F. Trevisan. IEEE Transactions on Magnetics, **51** (3), 1–4 (2015). DOI: 10.1109/TMAG.2014.2358701
[17] G. Xu, J. Zhang, X. Zang, O. Sugihara, H. Zhao, and Bin Cai. Optics Express, **24** (20), 23177–23185 (2016). DOI: 10.1364/OE.24.023177
[18] N.M. Ushakov, I.D. Kosobudskiy, M.Y. Vasilkov. J. Optics and Photonics Res., 1–12 (2025). DOI: 10.47852/bonviewJOPR52025894

Translated by M.Verenikina